Engineering 2 (2016) 132–140

Contents lists available at ScienceDirect

Engineering

journal homepage: www.elsevier.com/locate/eng

Research
Pharmaceutical Engineering—Review

Tumor Molecular Imaging with Nanoparticles

Zhen Cheng [a], Xuefeng Yan [b,c], Xilin Sun [b,c], Baozhong Shen [b,c,*], Sanjiv Sam Gambhir [a,d,*]

[a] Molecular Imaging Program at Stanford, Department of Radiology, Stanford University, Stanford, CA 94305, USA
[b] Molecular Imaging Research Center of Harbin Medical University, Harbin 150001, China
[c] TOF-PET/CT/MR Center, the Fourth Hospital of Harbin Medical University, Harbin 150001, China
[d] Departments of Bioengineering & Materials Science and Engineering, Bio-X Program, Canary Center at Stanford for Cancer Early Detection, Stanford University, Stanford, CA 94305, USA

ARTICLE INFO

Article history:
Received 5 January 2016
Revised 7 March 2016
Accepted 9 March 2016
Available online 31 March 2016

Keywords:
Tumor
Molecular imaging
Nanoparticles

ABSTRACT

Molecular imaging (MI) can provide not only structural images using traditional imaging techniques but also functional and molecular information using many newly emerging imaging techniques. Over the past decade, the utilization of nanotechnology in MI has exhibited many significant advantages and provided new opportunities for the imaging of living subjects. It is expected that multimodality nanoparticles (NPs) can lead to precise assessment of tumor biology and the tumor microenvironment. This review addresses topics related to engineered NPs and summarizes the recent applications of these nanoconstructs in cancer optical imaging, ultrasound, photoacoustic imaging, magnetic resonance imaging (MRI), and radionuclide imaging. Key challenges involved in the translation of NPs to the clinic are discussed.

1. Introduction

Cancer is now the leading cause of death in the world [1]. China constitutes approximately 20% of the world's population, and comprises 29.42% of new cancer cases and 27% of cancer deaths worldwide. In 2012, the cancer incidence rate in China was 1.74%, and the cancer mortality rate was 1.22%. In China, cancers of the stomach and liver have traditionally occurred with the highest frequency; however, the incidence of lung cancer has increased as the leading cause of cancer in recent years [2]. Despite the fact that huge advances in diagnostic technologies have led to an explosion of knowledge in cancer research, only a minute number of cancer patients are diagnosed at early stages due to the poor selectivity and sensitivity of conventional diagnostic techniques.

Traditional imaging technologies reflect mostly anatomical changes that differentiate pathological from normal tissue rather than measuring the biological processes responsible for disease. Molecular imaging (MI) is a rapidly emerging biomedical research method that enables visual representation, characterization, and quantification of biological processes at the cellular and/or molecular level within living organisms [3–5]. Several MI modalities are currently available, including fluorescence and bioluminescence imaging, targeted ultrasound (US), molecular magnetic resonance imaging (MRI), magnetic resonance spectroscopy (MRS), single-photon-emission computed tomography (SPECT), and positron emission tomography (PET). Probes or beacons, which can accumulate at the site of interest and allow for imaging, are required for MI. However, the limitations of some MI techniques include poor spatial resolution, low sensitivity, or poor signal penetration through tissues. For example, optical imaging is restricted in its depth-penetration capability, leading to poorer resolution, whereas MRI can image deep tissues but is much less sensitive (Table 1).

Nanoparticles (NPs) are emerging as a new class of MI agent to overcome these major hurdles in detecting human disease. NPs have great potential for accurate cancer diagnosis via passive accumulation and/or active-targeting approaches [6]. Combining

* Corresponding authors
E-mail addresses: sgambhir@stanford.edu; shenbzh@vip.sina.com

http://dx.doi.org/10.1016/J.ENG.2016.01.027

Table 1
Molecular imaging modalities.

Modality	Form of energy used	Spatial resolution (mm)	Advantages	Imaging cost	Clinical translation
Fluorescence imaging	Visible to infrared light	< 1 (fluorescence reflectance imaging, FRI); 1 (fluorescence molecular tomography, FMT)	High sensitivity; multiplexed imaging	Low (FRI); medium-high (FMT)	Yes
Bioluminescence imaging	Visible to infrared light	3–5	High sensitivity; high-throughput	Low	No
Ultrasound (US)	High frequency sound waves	0.04–0.1 (small-animal US); 0.1–1 (clinical US)	High sensitivity; portable	Low-medium	Yes
Positron emission tomography (PET)	Annihilation photos	1–2 (micro PET); 6–10 (clinical PET)	High sensitivity; quantitative; tracer amount of probe	High	Yes
Single-photon-emission computed tomography (SPECT)	Gamma rays	0.5–2 (micro SPECT); 7–15 (clinical SPECT)	High sensitivity; quantitative; tracer amount of probe	Medium-high	Yes
Magnetic resonance imaging (MRI)	Radio frequency waves	0.01–0.1 (small-animal MRI); 0.5–1.5 (clinical MRI)	High sensitivity; quantitative; tracer amount of probe	High	Yes

their large payload-carrying capacity, high signal intensity, and stability, NPs can deliver high concentrations of imaging agents to the target region. NPs are typically smaller than cells [7], and are comparable in size to molecules and proteins [8].

Historically, many of the developed NPs are considered to accumulate in tumors based on the enhanced permeability and retention (EPR) effect, which in nanomedicine research has been considered a universal feature of solid malignant tumors that can serve as the basis for passive tumor-targeting by therapeutic and diagnostic NPs [9–17]. The EPR effect was first reported as a concept of the delivery of macromolecular drugs to tumors [18]. However, the heterogeneity of the EPR effect provoked a debate about the real value of this effect. Many experimental scientists, pharmacologists, and nanotechnology engineers hold to the premise that solid tumors consist of uniform tissue; that is, that tumors are homogeneous [19]. However, as this is not the case, new strategies such as active targeted NPs have been pursued. Targeted NPs can perform with both high sensitivity and specificity to achieve high accumulation at the tumor site [20–23]. Active targeting requires the therapeutic agent to be guided to the target by conjugating the therapeutic agent or carrier system to a tissue or cell-specific ligand. In addition, using targeted NPs with a variety of moieties to reach multiple binding sites can provide higher binding efficiencies for targeting specific tumor sites.

A number of articles review the current applications of nanotechnologies for MI [24]. This paper presents a brief overview of recent developments in nanotechnology for MI, and will also address the drawbacks and future challenges of current nanoplatforms for the clinical translation of imaging.

2. Nanoplatforms

A wealth of NP-based systems exploits nanoplatforms for many imaging modalities. These NPs come in a wide variety of compositions, sizes, shapes, and structures from a variety of materials [25,26]. These different materials and shapes range from spheres, rods, and cubes to resembling snowflakes, flowers, thorns, hemispheres, worms, discoids, and chains—a wide variety that enables many imaging modalities (e.g., optical imaging, MRI, US, and/or nuclear imaging) for combining disease diagnosis and therapy into so-called "theranostic" (therapy plus diagnostic) applications. As mentioned earlier, NPs have been known to target tumors via passive- and/or active-targeting pathways. Due to abnormally leaky vasculature and the lack of an effective lymphatic drainage system in tumor tissues, NP platforms can passively accumulate in tumor tissues. These unique phenomena are jointly referred to as the EPR effect. Moreover, NPs can recognize, bind to, and internalize into tumor cells via receptor-mediated endocytosis when modified with tumor-targeting moieties such as antibodies, nucleic acids, proteins, or other ligands. In this section, we will describe exemplary theranostic nanoplatforms along with their applications regarding cancer.

2.1. Optical nanoparticles

Optical imaging offers high sensitivity, cost-effectiveness, non-ionizing radiation, and great potential for small-animal studies. However, the penetration depth of light prohibits deep-tissue imaging and is the major disadvantage for *in vivo* imaging in humans; thus, optical imaging is typically not quantitative for living-subject imaging studies. An abundance of probes, including synthetic fluorophores, semiconductor fluorescent crystals, and probes based on lanthanide rare-earth ions, have been developed for small-animal imaging [27–29].

Quantum dots (QDs) are the most widely studied NPs for preclinical optical imaging applications. Compared with organic fluorophores, QDs possess many superior properties for biological imaging, such as a strong resistance to photobleaching and chemical degradation, high quantum yields, continuous absorption spectra from ultraviolet (UV) to near-infrared (NIR), and large effective Stokes shifts [30–33]. Arginine-glycine-aspartic acid (RGD)-QDs could selectively bind to luminal endothelium in mouse tumor neovasculature [34]. However, because of their small size, QDs demonstrated poor retention inside the tumor, easily washing back out into the bloodstream [33] (Fig. 1). Nevertheless, the major drawbacks for the clinical utility of QDs are their potential toxicity and lack of deep-tissue imaging and quantification ability [35]. With the help of small-animal PET, radiolabeled QDs were found to have rapid uptake into the reticuloendothelial system (RES), liver, and spleen [36,37]. In order to reduce the uptake of QDs into the RES, human serum albumin (HSA) was explored as a coating for QD800-mercaptopropionic acid (MPA) NPs. The resulting QD800-MPA-HSA NPs show reduced localization in mononuclear phagocytic system-related organs over QD800-MPA, plausibly due to the low uptake of QD800-MPA-HSA in macrophage cells. QD800-MPA-HSA may have great potential for *in vivo* fluorescence imaging [38]. Affibody-modified QDs also showed high specificity for targeting human epidermal growth factor receptor 2 (HER2)-expressing cells and tumors [39].

Dyes that can be incorporated or encapsulated in polymeric NPs include indocyanine green (ICG) [40], NIR region fluorescent cyanine 7 (Cy7) [41], and dialkylcarbocyanine fluorophores [42], which have been approved by the United States Food and Drug Administration (FDA). A nanoplatform strategy is a promising method to enable optical imaging to overcome the drawbacks of free and small dyes [43,44]. Various nanocarriers have been investigated for the delivery of NIR dye to tumor sites, including liposomes, silica, polymersomes, and targeted rare-earth nano-

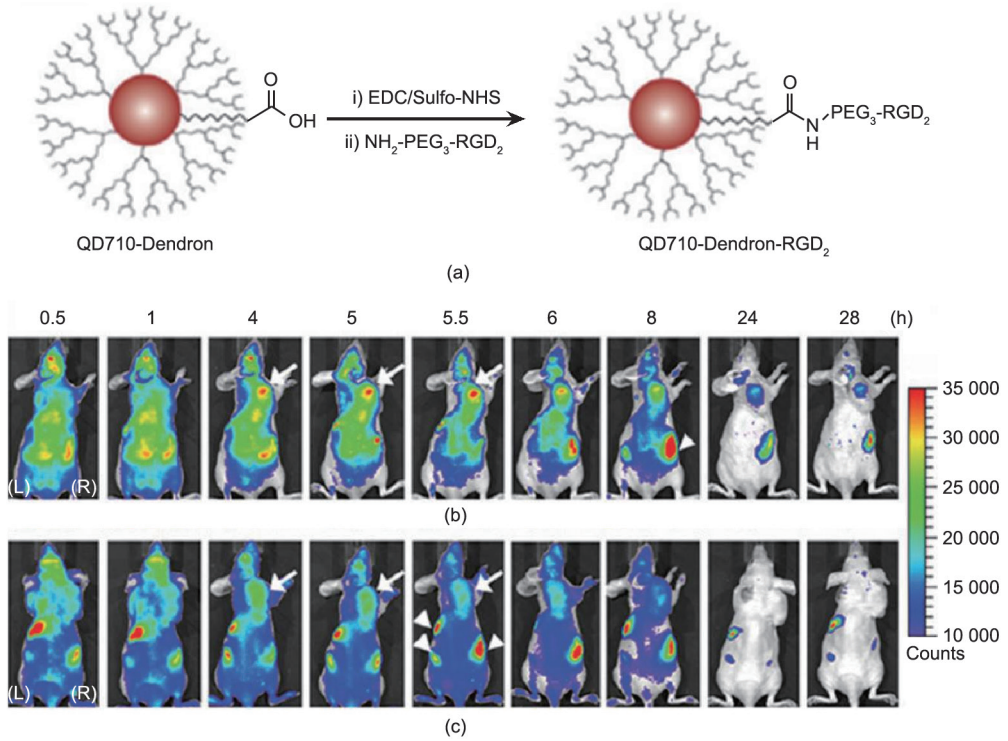

Fig. 1. (a) Structure and synthesis of QD710-Dendron-RGD_2 conjugate. QD710-Dendron with carboxylate terminal group was conjugated with RGD dimer by carbodiimide coupling. *In vivo* near-infrared fluorescence imaging. The dorsal images of SKOV3 tumor-bearing (arrows) mice (L, left side; R, right side) injected with (b) QD710-Dendorn-RGD_2 (200 pmol) and (c) QD710-Dendron (200 pmol) at 0.5 h, 1 h, 4 h, 5 h, 5.5 h, 6 h, 8 h, 24 h, and 28 h, respectively. The incidental high fluorescent signals in other body parts (arrowheads) might have originated from regular rodent food in stomach and feces in intestine. Adapted with permission from Gao et al. [33], © 2012 American Chemical Society.

crystals [45].

To overcome the light penetration issue and realize deep-tissue imaging, radiation-luminescence-excited fluorophores such as QDs can be used for *in vivo* multiplexed optical imaging by mimicking a natural bioluminescence resonance energy transfer (BRET) process, in which chemical energy is converted into photons to excite the QDs [46]. Photocaged upconversion nanoparticles (UCNPs) take advantage of the photon upconversion of NIR light to UV light to trigger the uncaging of *D*-luciferin from *D*-luciferin-conjugated UCNPs. The released *D*-luciferin effectively confers enhanced fluorescence and bioluminescence signals *in vitro* and *in vivo*, with deep light penetration and low cellular damage [47].

Cerenkov luminescence imaging is an emerging imaging modality, similar to bioluminescence imaging, which captures visible photons emitted by Cerenkov radiation [48]. Radioluminescent nanophosphors (RLNPs) have been proposed as MI probes in the development of combined X-ray/optical imaging modalities, such as X-ray luminescence computed tomography (XLCT) [49–51]. PEGylated Eu^{3+}-doped nanophosphors under biological conditions were shown to emit luminescence under excitation by either ^{18}F radioisotope or X-rays. This capability provides the potential to enable novel imaging modalities, such as XLCT or deep-tissue Cerenkov luminescence imaging [52].

Raman spectroscopy is based on the light-scattering phenomenon, as opposed to the absorption/emission in fluorescence, and Raman active molecules are more photostable than fluorophores, which are rapidly photobleached. Surface-enhanced Raman spectroscopy (SERS), active NPs, and single-wall nanotubes (SWNTs) can be used for noninvasive imaging in small living subjects by using Raman spectroscopy [53,54]. Affibody-functionalized gold silica NPs performed Raman MI of the epidermal growth factor receptor in a colon cancer mouse model [55].

Photoacoustic imaging (PAI) is a new hybrid biomedical imaging modality related to optical imaging, which has the potential for both functional and anatomic imaging [56]. The generated ultrasonic waves are detected by ultrasonic transducers and then analyzed to produce images. However, exogenous contrast agents are needed for MI, due to the differences in the absorption spectra of different tissues [57]. Non-plasmonic or plasmonic NPs, such as gold nanoshells, nanorods, or nanocages, can promote light absorption, improving the contrast of PAI signals [58]. Perylene-diimide (PDI)-based NIR-absorptive organic NPs (micelle-enveloped PDI) are an efficient contrast agent for the PAI of deep brain tumors in living mice. By encapsulating them into amphiphilic molecules, water-soluble PDI NPs were easily synthesized and exhibited excellent PAI properties [59]. PAI of targeted SWNTs may contribute to the noninvasive cancer imaging and monitoring of nanotherapeutics in living subjects [60–63]. Melanin nanoparticle (MNP) is another biopolymer with good biocompatibility and biodegradability, intrinsic photoacoustic (PA) properties, and binding ability to drugs, as an efficient endogenous nanosystem for imaging-guided chemotherapy [64,65]. Sorafenib (SRF) is chosen for constructing PEGylated-melanin-drug system. SRF-PEG-MNPs were labeled with ^{64}Cu and used to perform a PET/PAI dual modalities imaging-guided therapy [66]. By embedding ultrasmall MNPs into the cavities of apoferritin (APF), nanomaterials apoferritin-melanin-Fe (AMF) NPs with core-shell structures can easily load $^{64}Cu^{2+}$ and Fe^{3+} to achieve trimodal (PET/MRI/PAI) imaging [67] (Fig. 2).

2.2. Ultrasound agents

US has excellent spatial resolution and contrast sensitivity. Due to its low cost and wide availability, US is the most common-

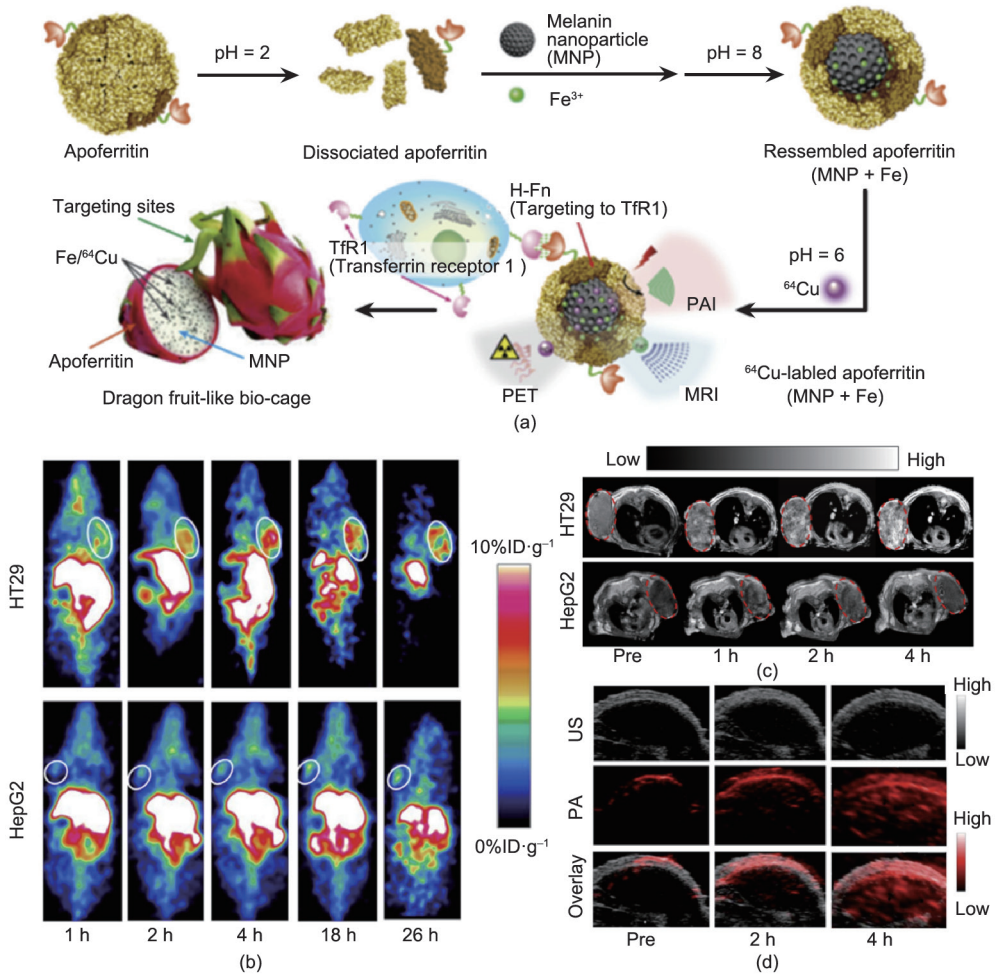

Fig. 2. (a) Schematic illustration of AMF nanocage synthesis. (b) Representative coronal small animal PET images of HT29 (top) and HepG2 (bottom) tumor-bearing mice (n = 4) at 1 h, 2 h, 4 h, 18 h, and 26 h after administration of ^{64}Cu-AMF. White circles indicate tumor location. (c) $T1$ magnetic resonance images of HT29 (upper) and HepG2 (lower) tumor model after administration of AMF, red circles indicate the area of tumor. (d) The ultrasound (grey, top), photoacoustic (red, middle) and overlayed coronal sections (bottom) of HT29 tumor models before and after tail-vein injection of AMF nanocages. Adapted with permission from Yang et al. [67], © 2015, Elsevier Ltd.

ly used clinical imaging modality [68]. Its use is limited in the imaging of some organs, such as lungs. Nanoscale US agents have been reported in the past decade [69,70]. A strategy to improve the *in vivo* half-life of US agents has been explored by targeting vascular markers of tumor angiogenesis [71]. While there have been recent examples of nanoscale US agents, due to the short *in vivo* half-life of US agents, the vast majority of targeted agent development has focused on seeking vascular markers of tumor angiogenesis. Anderson et al. [72] modified the surface of microbubbles (MBs) with cRGD ligand and then showed that these exhibit five-fold higher adhesion to immobilized recombinant $\alpha_v\beta_3$ integrin, compared with control groups. Yan et al. [73] synthesized iRGD-lipopeptides into an MB membrane. The binding specificity of iRGD-MBs for endothelial cells was found to be significantly stronger than that of control MBs under *in vitro* static and dynamic conditions. Furthermore, many peptides have been developed as ligands to direct MBs to integrins. Willmann et al. [74] designed MBs with engineered cystine knot (knottin) peptides, a new class of targeting ligands to $\alpha_v\beta_3$ integrin, for targeted contrast-enhanced US imaging of tumor angiogenesis. MB-Knottin$_{Integrin}$ attached significantly more to $\alpha_v\beta_3$ integrin positive cells than to control cells. In addition to integrins, the expression of vascular endothelial growth factor receptor 2 (VEGFR2) is another target of interest for imaging and monitoring during treatment. Contrast agent MBs for dual-targeting imaging can be modified to attach to both VEGFR2 and $\alpha_v\beta_3$ integrin [75]. As a result of the increased avidity that comes from the multi-ligand approach, the dual-targeting US MBs exhibited significantly higher signal compared with the single-targeting counterparts.

2.3. Magnetic nanoparticles

MRI is a noninvasive diagnostic technique providing superb image resolution and exquisite soft-tissue contrast for anatomical details. A considerable amount of work has been done in the development of MRI NPs, and especially with iron oxide NPs (IONPs). This is an important class of nanoplatform with the advantages of high sensitivity, shortened $T1$ and $T2$ relaxation times in a dose-dependent manner, and the versatility to present a wide variety of ligands for cellular and molecular imaging. There are more than 20 current clinical trials of superparamagnetic iron oxide (SPIO) or ultrasmall superparamagnetic iron oxide (USPIO). The iron oxide NPs are usually taken up by the RES [76], which also permits liver [77–79], spleen [80], and lymph node imaging. The accumulation of these NPs at the tumor site is based on the EPR effect due to the presence of leaky vasculature as well as uptake by macrophages.

IONPs such as SPIO NPs have been extensively studied for

tumor-targeting probes due to their excellent biocompatibility [10]. The synthesis process for these particles ranges from traditional wet chemistry solution-based methods to more exotic techniques [81,82]. The field of magnetic NP probe technology has recently been promoted by efforts devoted to developing its potential as an important tool for efficient cross-application MI [83]. Hybrid nanotrimers performed dual *T*1- and *T*2-weighted MRI with high accuracy and reliability, as revealed by a PET imaging study, and displayed favorable biodistribution and suitability for *in vivo* imaging [84] (Fig. 3).

Research with SPIO NPs has already demonstrated their utility as an important tool for enhancing magnetic resonance (MR) contrast [85]. It is desirable for the NPs used for this application to have high magnetization values and a size smaller than 100 nm, with a narrow particle-size distribution [86]. Magnetic NPs offer a number of advantages, including laser-induced thermal therapy, the ability to target specific sites, and relatively low toxicity [87]. Biological applications of magnetic NPs also require magnetic particles to have a special surface coating that must be nontoxic and biocompatible, and that must permit targetable delivery with particle localization in a specific area. Such magnetic NPs can be easily conjugated to drugs, proteins, enzymes, antibodies, or nucleotides and can be directed to an organ, tissue, or tumor using an external magnetic field.

The specific structure of dendrimers makes them an attractive NP platform for gadolinium (Gd)-loading due to their narrow size distribution (5–10 nm); branched structure, which facilitates the presentation of multiple ligands or contrast agents; and associated renal clearance. For example, Gd-loaded dendrimers targeting the folate receptor displayed enhanced MR signal in an animal model of a κB-tumor. When designing Gd-based agents, several factors need to be considered, since signal intensity at the target site is not linearly related to the concentration of the imaging moiety. For example, the intracellular accumulation of Gd can markedly impact signal intensity. Furthermore, the presence of Gd atoms in an NP structure also impacts the efficiency of NP MR probes.

2.4. Nanoparticles for nuclear imaging

With the development of the micro scanner contributing to small-animal imaging, nuclear imaging can be performed with low mass amounts to measure the function of biological processes [88]. With high contrast sensitivity, PET imaging plays an important role in MI, albeit with the disadvantage of low resolution. Based on existing knowledge of nuclear imaging with small molecules, NP-based nuclear imaging agents have been rapidly developed. During the past decade, there have been various reports on PET imaging with targeted NPs. The most common way to integrate PET imaging capability into NPs is to attach a radiometal (e.g., ^{64}Cu) via a metal chelator, such as 1,4,7,10-tetraazacyclododecanetetraacetic acid (DOTA) or 1,4,7-triazacyclononane-*N*,*N*′,*N*″-triacetic acid (NOTA). After purification, NPs radiolabeled with ^{64}Cu can reach greater than 95% radiochemical purity [89–91].

Since no single modality is perfect and sufficient to obtain all necessary information, several other NP platforms have been investigated for the development of multimodal contrast agents, such as for use with combined PET and optical imaging, or PET and MRI. Multimodal imaging enables the use of PET for treatment planning with whole-body imaging, and the use of optical techniques during therapeutic intervention. Cai et al. [92] developed a near-infrared fluorescence (NIRF) imaging and PET imaging agent based on QD. RGD peptides were modified on the

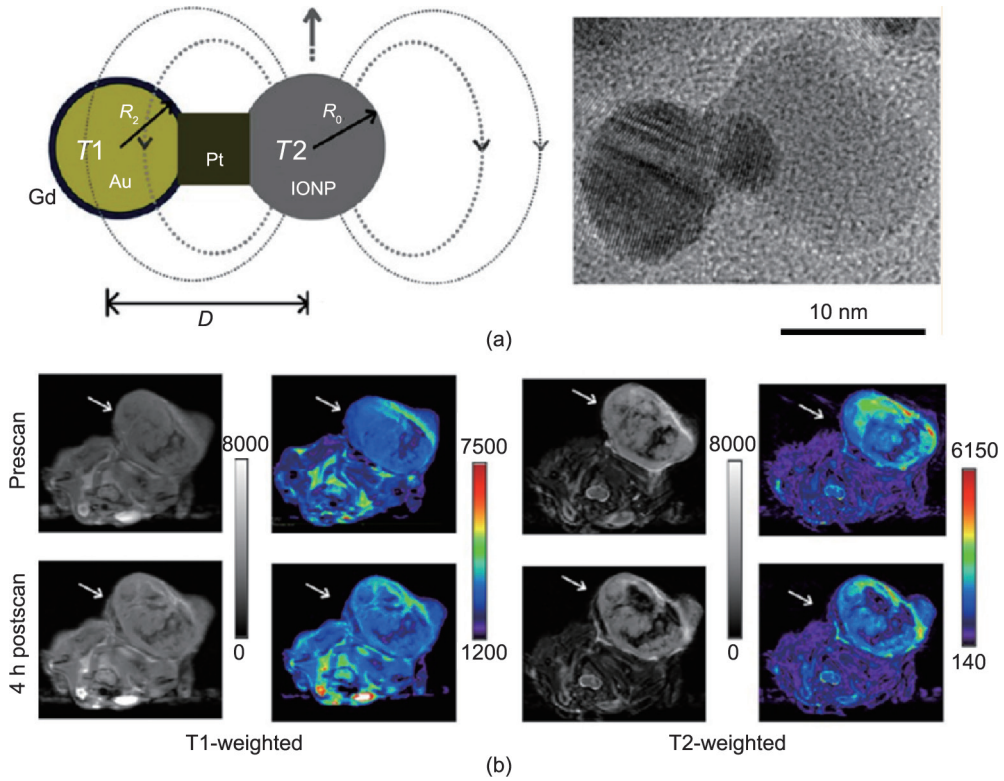

Fig. 3. (a) Engineering the heterogeneous nanostructures for magnetic coupling of *T*1 and *T*2 contrast agents (left) and transmission electron microscope (TEM) image of dumbbell structure (right). (b) *T*1- and *T*2-weighted magnetic resonance images of HT29 tumor bearing mice (n = 3) before and after intravenous injection of Gd-DB-HNTs. The left ones show gray scale images, and the right ones show the pseudocolored images. Adapted with permission from Cheng et al. [84], © 2014 American Chemical Society.

surface of QDs, allowing them to target the $\alpha_v\beta_3$ integrin. At the same time, DOTA was also conjugated for ^{64}Cu labeling. This dual-modality probe sufficiently improves tumor contrast while decreasing the dose required for *in vivo* NIRF imaging, thus leading to a significant reduction in the potential toxicity of QDs [93,94]. Similarly, Chen et al. [95] synthesized a ^{64}Cu-DOTA-QD-VEGF nanoprobe to primarily target the vasculature through a VEGF-VEGFR interaction. Nahrendorf et al. [96,97] synthesized a dextran-coated SPIO NP co-labeled with ^{64}Cu and an NIR fluorophore (VivoTag 680), which can perform both fluorescence molecular tomography (FMT) and PET imaging of tumor-associated macrophages. Yang et al. [98] modified a multimodal RGD-targeted SPIO. After labeling with ^{64}Cu, the NPs can be used for monitoring drug delivery to solid tumors through PET/MR dual-modal imaging [98]. As a photosensitizer, porphyrin not only provides photodynamic ability but also serves as a promising dye for fluorescent imaging. Liu et al. [99] developed a ^{64}Cu-porphorysome nanoplatform presenting the ability to detect small bone metastases in lower limbs through optical-PET dual-modal imaging. Chen et al. [100] recently investigated targeted hollow mesoporous silica NPs (HMSNs) for PET/optical imaging of tumor angiogenesis by using CD105. They demonstrated a three-fold higher accumulation compared with their non-targeted group [100] (Fig. 4). Liu et al. [61] investigated integrin-targeted SWNTs, which performed remarkable dual Raman and PET tumor-targeting imaging. Zirconium-89 (^{89}Zr) is a new and promising PET radionuclide for *in vivo* studies [101–105]. Ruggiero et al. [106] developed antibody-labeled ^{89}Zr-SWNT, which targeted the monomeric vascular endothelial-cadherin (VE-cad) epitope with monitoring by PET and NIRF imaging. Using this nanoplatform, the tumor angiogenesis can be estimated. Lee et al. [107] monodispersely synthesized polymer-coated UCNPs and dimeric RGD-conjugated UCNPs. This NP platform can be used for optical imaging, MRI, and PET, with highly selective targeting to $\alpha_v\beta_3$ integrin [107]. Lijowski et al. [108] designed *T*1-based $\alpha_v\beta_3$-targeted ^{99m}Tc-Gd NPs, which produced high sensitivity and specific localization of tumor angiogenesis by SPECT-MR imaging [108]. Hu et al. [109] investigated ^{111}In-perfluorocarbon modified by $\alpha_v\beta_3$ integrin, producing a multimodal PET-MR agent. Radiolabeling Ac-Cys-ZEGFR:1907-modified Au-IONP (NOTA-Au-IONP-affibody) with PET radionuclide, ^{64}Cu, resulted in an epidermal growth factor receptor (EGFR)-targeted PET/optical/MR imaging probe, ^{64}Cu-NOTA-Au-IONP-affibody, targeted toward EGFR-positive tumors [110].

3. Challenges and future perspectives

Some fundamental hurdles hamper the approval of NPs for clinical use; these hurdles correlate to various materials characteristics including size, shape, composition, single crystallinity, and magnetism. The first hurdle is that of delivery obstacles. In particular, the RES can phagocytose the NPs, rapidly sweeping them out of blood circulation and accumulating them in the liver, spleen, and bone marrow. This phenomenon gives cause to further toxicity concerns. The toxicity of NPs is another very important hurdle. Toxicity can result not only from concentration in the bone marrow and other organs but also from the composition of the NPs themselves, such as the Cd used in QDs and other coating materials. Additional hurdles include the inability to overcome certain biological barriers, such as the blood-brain barrier (BBB), as well as the lack of control over the distribution of NPs following administration. The fate of NPs after their intravenous administration is highly variable and dependent on their size, morphology, charge, and surface chemistry. An NP size of below 100 nm is often used in order to increase effectiveness and blood-circulation time, for adequate exposure to the tumor and drug release.

Given these existing hurdles, next-generation platforms will likely emphasize the development of small-size NPs, their high

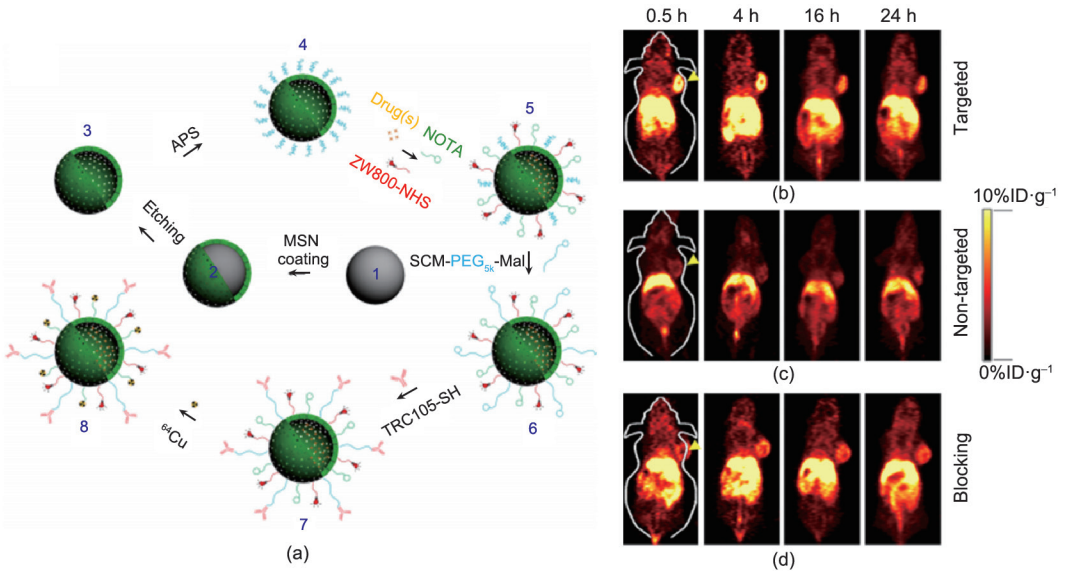

Fig. 4. (a) Surface engineering of HMSN. Uniform dense silica ($dSiO_2$, 1) was firstly synthesized and coated with a shell of MSN, forming $dSiO_2$@MSN (2). Tightly-controlled Na_2CO_3 etching step was introduced to selectively etch $dSiO_2$ away, leaving uniform HMSN (3). As-synthesized HMSN was then surface modified with (3-aminopropyl)triethoxysilane (APS) to form amino groups conjugated HMSN-NH_2 (4) before further bio-conjugations. Anticancer drugs (i.e., doxorubicin, DOX) were then loaded, followed by NIR dye (i.e., ZW800) and ^{64}Cu chelator (i.e., NOTA) conjugations, forming NOTA-HMSN(DOX)-ZW800 (5). Afterward, nano-conjugate was PEGylated with SCM-PEG_{5k}-Mal to render its stability in biological buffers (e.g., phosphate buffered saline, PBS), forming NOTAHMSN(DOX)-ZW800-PEG-Mal (6). Then, thiolated anti-CD105 antibody (i.e., TRC105-SH) was conjugated to the NP to obtain NOTAHMSN(DOX)-ZW800-PEG-TRC105 (7). Lastly, PET isotope ^{64}Cu ($t_{\frac{1}{2}}$ = 12.7 h) was used to label the NP, forming ^{64}Cu-NOTAHMSN(DOX)-ZW800-PEG-TRC105 (8). *In vivo* tumor targeted PET imaging. Serial coronal PET images of 4T1 tumor-bearing mice at different time points post-injection of (b) targeted group: ^{64}Cu-HMSN-ZW800-TRC105, (c) non-targeted group: ^{64}Cu-HMSN-ZW800, or (d) blocking group: ^{64}Cu-HMSN-ZW800-TRC105 with a blocking dose (1 mg per mouse) of free TRC105. Tumors were indicated by yellow arrowheads. Adapted with permission from Chen et al. [100], © 2014 Nature Publishing Group.

colloidal composition, and bio-stability. Significant improvements in sensitivity and target specificity are expected, which will bring huge advancements in current cancer-diagnostic capabilities. Additional regulatory and development considerations will arise when future generic nanomedicines are presented for health authority (FDA) approval with claims of equivalence to the innovator drug. In addition, in the face of the natural biological barriers to the delivery of nanomedicines, tissues with aberrant pathology, such as tumors, are often very efficient in harnessing active biological mechanisms for high nutrient supply and rapid growth. Elucidation of these active transport mechanisms and the ability to harness them with nanomedicines could provide a step forward in the treatment of cancer and other diseases.

4. Conclusions

Over the last decade, the field of nanotechnology has experienced tremendous growth and advancement. With substantial efforts by both researchers and the biopharmaceutical industry, a few nanomedicines have already been successfully approved for preclinical and clinical studies. However, the field of nanomedicine is still in its early stages due to unfamiliar types of risk in safety and efficacy that require further discussion and cooperation among researchers and governmental agencies. The challenges in developing NPs for use in MI may be overcome in the near future.

Compliance with ethics guidelines

Zhen Cheng, Xuefeng Yan, Xilin Sun, Baozhong Shen, and Sanjiv Sam Gambhir declare that they have no conflict of interest or financial conflicts to disclose.

References

[1] Torre LA, Bray F, Siegel RL, Ferlay J, Lortet-Tieulent J, Jemal A. Global cancer statistics, 2012. CA Cancer J Clin 2015;65(2):87–108.
[2] Yu S, Yang CS, Li J, You W, Chen J, Cao Y, et al. Cancer prevention research in China. Cancer Prev Res (Phila) 2015;8(8):662–74.
[3] Adams JY, Johnson M, Sato M, Berger F, Gambhir SS, Carey M, et al. Visualization of advanced human prostate cancer lesions in living mice by a targeted gene transfer vector and optical imaging. Nat Med 2002;8(8):891–7.
[4] Massoud TF, Gambhir SS. Molecular imaging in living subjects: seeing fundamental biological processes in a new light. Genes Dev 2003;17(5):545–80.
[5] James ML, Gambhir SS. A molecular imaging primer: modalities, imaging agents, and applications. Physiol Rev 2012;92(2):897–965.
[6] Koo H, Huh MS, Sun IC, Yuk SH, Choi K, Kim K, et al. In vivo targeted delivery of nanoparticles for theranosis. Acc Chem Res 2011;44(10):1018–28.
[7] Wiwanitkit V. Glomerular pore size corresponding to albumin molecular size, an explanation for underlying structural pathology leading to albuminuria at nanolevel. Ren Fail 2006;28(1):101.
[8] Ullman EF, Schwarzberg M, Rubenstein KE. Fluorescent excitation transfer immunoassay. A general method for determination of antigens. J Biol Chem 1976;251(14):4172–8.
[9] Heath JR, Davis ME. Nanotechnology and cancer. Annu Rev Med 2008;59:251–65.
[10] Ferrari M. Cancer nanotechnology: opportunities and challenges. Nat Rev Cancer 2005;5(3):161–71.
[11] Lammers T. Drug delivery research in Europe. J Control Release 2012;161(2):151.
[12] Brambilla D, Luciani P, Leroux JC. Breakthrough discoveries in drug delivery technologies: the next 30 years. J Control Release 2014;190:9–14.
[13] Taurin S, Nehoff H, Greish K. Anticancer nanomedicine and tumor vascular permeability; Where is the missing link? J Control Release 2012;164(3):265–75.
[14] Maeda H, Nakamura H, Fang J. The EPR effect for macromolecular drug delivery to solid tumors: improvement of tumor uptake, lowering of systemic toxicity, and distinct tumor imaging in vivo. Adv Drug Deliv Rev 2013;65(1):71–9.
[15] Altundag K, Dede DS, Purnak T. Albumin-bound paclitaxel (ABI-007; Abraxane) in the management of basal-like breast carcinoma. J Clin Pathol 2007;60(8):958.
[16] Chakravarthy AB, Kelley MC, McLaren B, Truica CI, Billheimer D, Mayer IA, et al. Neoadjuvant concurrent paclitaxel and radiation in stage II/III breast cancer. Clin Cancer Res 2006;12(5):1570–6.
[17] Maeda H, Wu J, Sawa T, Matsumura Y, Hori K. Tumor vascular permeability and the EPR effect in macromolecular therapeutics: a review. J Control Release 2000;65(1–2):271–84.
[18] Matsumura Y, Maeda H. A new concept for macromolecular therapeutics in cancer chemotherapy: mechanism of tumoritropic accumulation of proteins and the antitumor agent smancs. Cancer Res 1986;46(12 Pt 1):6387–92.
[19] Maeda H. Toward a full understanding of the EPR effect in primary and metastatic tumors as well as issues related to its heterogeneity. Adv Drug Deliv Rev 2015;91:3–6.
[20] Al-Jamal WT, Kostarelos K. Liposomes: from a clinically established drug delivery system to a nanoparticle platform for theranostic nanomedicine. Acc Chem Res 2011;44(10):1094–104.
[21] Ambrogio MW, Thomas CR, Zhao YL, Zink JI, Stoddart JF. Mechanized silica nanoparticles: a new frontier in theranostic nanomedicine. Acc Chem Res 2011;44(10):903–13.
[22] Bardhan R, Lal S, Joshi A, Halas NJ. Theranostic nanoshells: from probe design to imaging and treatment of cancer. Acc Chem Res 2011;44(10):936–46.
[23] Ho D, Sun X, Sun S. Monodisperse magnetic nanoparticles for theranostic applications. Acc Chem Res 2011;44(10):875–82.
[24] Thakor AS, Gambhir SS. Nanooncology: the future of cancer diagnosis and therapy. CA Cancer J Clin 2013;63(6):395–418.
[25] Piner RD, Zhu J, Xu F, Hong S, Mirkin CA. “Dip-Pen” nanolithography. Science 1999;283(5402):661–3.
[26] Canelas DA, Herlihy KP, DeSimone JM. Top-down particle fabrication: control of size and shape for diagnostic imaging and drug delivery. Wiley Interdiscip Rev Nanomed Nanobiotechnol 2009;1(4):391–404.
[27] Key J, Leary JF. Nanoparticles for multimodal in vivo imaging in nanomedicine. Int J Nanomedicine 2014;9:711–26.
[28] He X, Wang K, Cheng Z. In vivo near-infrared fluorescence imaging of cancer with nanoparticle-based probes. Wiley Interdiscip Rev Nanomed Nanobiotechnol 2010;2(4):349–66.
[29] He X, Gao J, Gambhir SS, Cheng Z. Near-infrared fluorescent nanoprobes for cancer molecular imaging: status and challenges. Trends Mol Med 2010;16(12):574–83.
[30] Alivisatos P. The use of nanocrystals in biological detection. Nat Biotechnol 2004;22(1):47–52.
[31] Michalet X, Pinaud FF, Bentolila LA, Tsay JM, Doose S, Li JJ, et al. Quantum dots for live cells, in vivo imaging, and diagnostics. Science 2005;307(5709):538–44.
[32] Medintz IL, Uyeda HT, Goldman ER, Mattoussi H. Quantum dot bioconjugates for imaging, labelling and sensing. Nat Mater 2005;4(6):435–46.
[33] Gao J, Chen K, Luong R, Bouley DM, Mao H, Qiao T, et al. A novel clinically translatable fluorescent nanoparticle for targeted molecular imaging of tumors in living subjects. Nano Lett 2012;12(1):281–6.
[34] Smith BR, Cheng Z, De A, Koh AL, Sinclair R, Gambhir SS. Real-time intravital imaging of RGD-quantum dot binding to luminal endothelium in mouse tumor neovasculature. Nano Lett 2008;8(9):2599–606.
[35] Cai W, Hsu AR, Li ZB, Chen X. Are quantum dots ready for in vivo imaging in human subjects? Nanoscale Res Lett 2007;2(6):265–81.
[36] Schipper ML, Cheng Z, Lee SW, Bentolila LA, Iyer G, Rao J, et al. microPET-based biodistribution of quantum dots in living mice. J Nucl Med 2007;48(9):1511–8.
[37] Schipper ML, Iyer G, Koh AL, Cheng Z, Ebenstein Y, Aharoni A, et al. Particle size, surface coating, and PEGylation influence the biodistribution of quantum dots in living mice. Small 2009;5(1):126–34.
[38] Gao J, Chen K, Xie R, Xie J, Lee S, Cheng Z, et al. Ultrasmall near-infrared non-cadmium quantum dots for in vivo tumor imaging. Small 2010;6(2):256–61.
[39] Gao J, Chen K, Miao Z, Ren G, Chen X, Gambhir SS, et al. Affibody-based nanoprobes for HER2-expressing cell and tumor imaging. Biomaterials 2011;32(8):2141–8.
[40] DeCoste SD, Farinelli W, Flotte T, Anderson RR. Dye-enhanced laser welding for skin closure. Lasers Surg Med 1992;12(1):25–32.
[41] Gianella A, Jarzyna PA, Mani V, Ramachandran S, Calcagno C, Tang J, et al. Multifunctional nanoemulsion platform for imaging guided therapy evaluated in experimental cancer. ACS Nano 2011;5(6):4422–33.
[42] Santra S, Kaittanis C, Grimm J, Perez JM. Drug/dye-loaded, multifunctional iron oxide nanoparticles for combined targeted cancer therapy and dual optical/magnetic resonance imaging. Small 2009;5(16):1862–8.
[43] Yan X, Niu G, Lin J, Jin AJ, Hu H, Tang Y, et al. Enhanced fluorescence imaging guided photodynamic therapy of sinoporphyrin sodium loaded graphene oxide. Biomaterials 2015;42:94–102.
[44] Yan X, Hu H, Lin J, Jin AJ, Niu G, Zhang S, et al. Optical and photoacoustic dual-modality imaging guided synergistic photodynamic/photothermal therapies. Nanoscale 2015;7(6):2520–6.
[45] Luo S, Zhang E, Su Y, Cheng T, Shi C. A review of NIR dyes in cancer targeting and imaging. Biomaterials 2011;32(29):7127–38.
[46] Liu H, Zhang X, Xing B, Han P, Gambhir SS, Cheng Z. Radiation-luminescence-excited quantum dots for in vivo multiplexed optical imaging. Small 2010;6(10):1087–91.
[47] Yang Y, Shao Q, Deng R, Wang C, Teng X, Cheng K, et al. In vitro and in vivo uncaging and bioluminescence imaging by using photocaged upconversion

nanoparticles. Angew Chem Int Ed Engl 2012;51(13):3125–9.
[48] Mitchell GS, Gill RK, Boucher DL, Li C, Cherry SR. In vivo Cerenkov luminescence imaging: a new tool for molecular imaging. Philos Trans A Math Phys Eng Sci 2011;369(1955):4605–19.
[49] Carpenter CM, Sun C, Pratx G, Rao R, Xing L. Hybrid x-ray/optical luminescence imaging: characterization of experimental conditions. Med Phys 2010;37(8):4011–8.
[50] Pratx G, Carpenter CM, Sun C, Rao RP, Xing L. Tomographic molecular imaging of x-ray-excitable nanoparticles. Opt Lett 2010;35(20):3345–7.
[51] Pratx G, Carpenter CM, Sun C, Xing L. X-ray luminescence computed tomography via selective excitation: a feasibility study. IEEE Trans Med Imaging 2010;29(12):1992–9.
[52] Sun C, Pratx G, Carpenter CM, Liu H, Cheng Z, Gambhir SS, et al. Synthesis and radioluminescence of PEGylated Eu(3+) -doped nanophosphors as bioimaging probes. Adv Mater 2011;23(24):H195–9.
[53] Keren S, Zavaleta C, Cheng Z, de la Zerda A, Gheysens O, Gambhir SS. Noninvasive molecular imaging of small living subjects using Raman spectroscopy. Proc Natl Acad Sci USA 2008;105(15):5844–9.
[54] Zavaleta CL, Hartman KB, Miao Z, James ML, Kempen P, Thakor AS, et al. Preclinical evaluation of Raman nanoparticle biodistribution for their potential use in clinical endoscopy imaging. Small 2011;7(15):2232–40.
[55] Jokerst JV, Miao Z, Zavaleta C, Cheng Z, Gambhir SS. Affibody-functionalized gold-silica nanoparticles for Raman molecular imaging of the epidermal growth factor receptor. Small 2011;7(5):625–33.
[56] Grinvald A, Lieke E, Frostig RD, Gilbert CD, Wiesel TN. Functional architecture of cortex revealed by optical imaging of intrinsic signals. Nature 1986;324(6095):361–4.
[57] He Y, Tang Z, Chen Z, Wan W, Li J. A novel photoacoustic tomography based on a time-resolved technique and an acoustic lens imaging system. Phys Med Biol 2006;51(10):2671–80.
[58] Wang LV, Hu S. Photoacoustic tomography: in vivo imaging from organelles to organs. Science 2012;335(6075):1458–62.
[59] Fan Q, Cheng K, Yang Z, Zhang R, Yang M, Hu X, et al. Perylene-diimide-based nanoparticles as highly efficient photoacoustic agents for deep brain tumor imaging in living mice. Adv Mater 2015;27(5):843–7.
[60] Bianco A, Kostarelos K, Prato M. Applications of carbon nanotubes in drug delivery. Curr Opin Chem Biol 2005;9(6):674–9.
[61] Liu Z, Cai W, He L, Nakayama N, Chen K, Sun X, et al. In vivo biodistribution and highly efficient tumour targeting of carbon nanotubes in mice. Nat Nanotechnol 2007;2(1):47–52.
[62] De la Zerda A, Zavaleta C, Keren S, Vaithilingam S, Bodapati S, Liu Z, et al. Carbon nanotubes as photoacoustic molecular imaging agents in living mice. Nat Nanotechnol 2008;3(9):557–62.
[63] De la Zerda A, Liu Z, Bodapati S, Teed R, Vaithilingam S, Khuri-Yakub BT, et al. Ultrahigh sensitivity carbon nanotube agents for photoacoustic molecular imaging in living mice. Nano Lett 2010;10(6):2168–72.
[64] Ren G, Miao Z, Liu H, Jiang L, Limpa-Amara N, Mahmood A, et al. Melanin-targeted preclinical PET imaging of melanoma metastasis. J Nucl Med 2009;50(10):1692–9.
[65] Cheng Z, Mahmood A, Li H, Davison A, Jones AG. [^{99m}TcOAADT]-$(CH_2)_2$-NEt_2: a potential small-molecule single-photon emission computed tomography probe for imaging metastatic melanoma. Cancer Res 2005;65(12):4979–86.
[66] Zhang R, Fan Q, Yang M, Cheng K, Lu X, Zhang L, et al. Engineering melanin nanoparticles as an efficient drug-delivery system for imaging-guided chemotherapy. Adv Mater 2015;27(34):5063–9.
[67] Yang M, Fan Q, Zhang R, Cheng K, Yan J, Pan D, et al. Dragon fruit-like biocage as an iron trapping nanoplatform for high efficiency targeted cancer multimodality imaging. Biomaterials 2015;69:30–7.
[68] Bloch SH, Dayton PA, Ferrara KW. Targeted imaging using ultrasound contrast agents. Progess and opportunities for clinical and research applications. IEEE Eng Med Biol Mag 2004;23(5):18–29.
[69] Liu R, Tian B, Gearing M, Hunter S, Ye K, Mao Z. Cdk5-mediated regulation of the PIKE-A-Akt pathway and glioblastoma cell invasion. Proc Natl Acad Sci USA 2008;105(21):7570–5.
[70] Zhou J, Patel TR, Sirianni RW, Strohbehn G, Zheng MQ, Duong N, et al. Highly penetrative, drug-loaded nanocarriers improve treatment of glioblastoma. Proc Natl Acad Sci USA 2013;110(29):11751–6.
[71] Kiessling F, Huppert J, Zhang C, Jayapaul J, Zwick S, Woenne EC, et al. RGD-labeled USPIO inhibits adhesion and endocytotic activity of $\alpha_v\beta_3$-integrin-expressing glioma cells and only accumulates in the vascular tumor compartment. Radiology 2009;253(2):462–9.
[72] Anderson CR, Hu X, Zhang H, Tlaxca J, Declèves AE, Houghtaling R, et al. Ultrasound molecular imaging of tumor angiogenesis with an integrin targeted microbubble contrast agent. Invest Radiol 2011;46(4):215–24.
[73] Yan F, Xu X, Chen Y, Deng Z, Liu H, Xu J, et al. A lipopeptide-based $\alpha_v\beta_3$ integrin-targeted ultrasound contrast agent for molecular imaging of tumor angiogenesis. Ultrasound Med Biol 2015;41(10):2765–73.
[74] Willmann JK, Kimura RH, Deshpande N, Lutz AM, Cochran JR, Gambhir SS. Targeted contrast-enhanced ultrasound imaging of tumor angiogenesis with contrast microbubbles conjugated to integrin-binding knottin peptides. J Nucl Med 2010;51(3):433–40.
[75] Willmann JK, Lutz AM, Paulmurugan R, Patel MR, Chu P, Rosenberg J, et al. Dual-targeted contrast agent for US assessment of tumor angiogenesis in vivo. Radiology 2008;248(3):936–44.
[76] Chavanpatil MD, Khdair A, Panyam J. Nanoparticles for cellular drug delivery: mechanisms and factors influencing delivery. J Nanosci Nanotechnol 2006;6(9-10):2651–63.
[77] Shamsi K, Balzer T, Saini S, Ros PR, Nelson RC, Carter EC, et al. Superparamagnetic iron oxide particles (SH U 555 A): evaluation of efficacy in three doses for hepatic MR imaging. Radiology 1998;206(2):365–71.
[78] Reimer P, Jähnke N, Fiebich M, Schima W, Deckers F, Marx C, et al. Hepatic lesion detection and characterization: value of nonenhanced MR imaging, superparamagnetic iron oxide-enhanced MR imaging, and spiral CT-ROC analysis. Radiology 2000;217(1):152–8.
[79] Bu L, Xie J, Chen K, Huang J, Aguilar ZP, Wang A, et al. Assessment and comparison of magnetic nanoparticles as MRI contrast agents in a rodent model of human hepatocellular carcinoma. Contrast Media Mol Imaging 2012;7(4):363–72.
[80] de Marco G, Bogdanov A, Marecos E, Moore A, Simonova M, Weissleder R. MR imaging of gene delivery to the central nervous system with an artificial vector. Radiology 1998;208(1):65–71.
[81] Gupta AK, Curtis AS. Surface modified superparamagnetic nanoparticles for drug delivery: interaction studies with human fibroblasts in culture. J Mater Sci Mater Med 2004;15(4):493–6.
[82] Akbarzadeh A, Samiei M, Davaran S. Magnetic nanoparticles: preparation, physical properties, and applications in biomedicine. Nanoscale Res Lett 2012;7(1):144.
[83] Thorek DL, Chen AK, Czupryna J, Tsourkas A. Superparamagnetic iron oxide nanoparticle probes for molecular imaging. Ann Biomed Eng 2006;34(1):23–38.
[84] Cheng K, Yang M, Zhang R, Qin C, Su X, Cheng Z. Hybrid nanotrimers for dual T_1 and T_2-weighted magnetic resonance imaging. ACS Nano 2014;8(10):9884–96.
[85] Yoffe S, Leshuk T, Everett P, Gu F. Superparamagnetic iron oxide nanoparticles (SPIONs): synthesis and surface modification techniques for use with MRI and other biomedical applications. Curr Pharm Des 2013;19(3):493–509.
[86] Gupta AK, Gupta M. Synthesis and surface engineering of iron oxide nanoparticles for biomedical applications. Biomaterials 2005;26(18):3995–4021.
[87] Yu MK, Jeong YY, Park J, Park S, Kim JW, Min JJ, et al. Drug-loaded superparamagnetic iron oxide nanoparticles for combined cancer imaging and therapy in vivo. Angew Chem Int Ed Engl 2008;47(29):5362–5.
[88] Phelps ME, Hoffman EJ, Huang SC, Ter-Pogossian MM. Effect of positron range on spatial resolution. J Nucl Med 1975;16(7):649–52.
[89] Shokeen M, Anderson CJ. Molecular imaging of cancer with copper-64 radiopharmaceuticals and positron emission tomography (PET). Acc Chem Res 2009;42(7):832–41.
[90] Cutler CS, Hennkens HM, Sisay N, Huclier-Markai S, Jurisson SS. Radiometals for combined imaging and therapy. Chem Rev 2013;113(2):858–83.
[91] Wadas TJ, Wong EH, Weisman GR, Anderson CJ. Coordinating radiometals of copper, gallium, indium, yttrium, and zirconium for PET and SPECT imaging of disease. Chem Rev 2010;110(5):2858–902.
[92] Cai W, Chen K, Li ZB, Gambhir SS, Chen X. Dual-function probe for PET and near-infrared fluorescence imaging of tumor vasculature. J Nucl Med 2007;48(11):1862–70.
[93] Kirchner C, Liedl T, Kudera S, Pellegrino T, Muñoz Javier A, Gaub HE, et al. Cytotoxicity of colloidal CdSe and CdSe/ZnS nanoparticles. Nano Lett 2005;5(2):331–8.
[94] Cai W, Shin DW, Chen K, Gheysens O, Cao Q, Wang SX, et al. Peptide-labeled near-infrared quantum dots for imaging tumor vasculature in living subjects. Nano Lett 2006;6(4):669–76.
[95] Chen K, Li ZB, Wang H, Cai W, Chen X. Dual-modality optical and positron emission tomography imaging of vascular endothelial growth factor receptor on tumor vasculature using quantum dots. Eur J Nucl Med Mol Imaging 2008;35(12):2235–44.
[96] Nahrendorf M, Zhang H, Hembrador S, Panizzi P, Sosnovik DE, Aikawa E, et al. Nanoparticle PET-CT imaging of macrophages in inflammatory atherosclerosis. Circulation 2008;117(3):379–87.
[97] Nahrendorf M, Keliher E, Marinelli B, Waterman P, Feruglio PF, Fexon L, et al. Hybrid PET-optical imaging using targeted probes. Proc Natl Acad Sci USA 2010;107(17):7910–5.
[98] Yang X, Hong H, Grailer JJ, Rowland IJ, Javadi A, Hurley SA, et al. cRGD-functionalized, DOX-conjugated, and ^{64}Cu-labeled superparamagnetic iron oxide nanoparticles for targeted anticancer drug delivery and PET/MR imaging. Biomaterials 2011;32(17):4151–60.
[99] Liu TW, Macdonald TD, Jin CS, Gold JM, Bristow RG, Wilson BC, et al. Inherently multimodal nanoparticle-driven tracking and real-time delineation of orthotopic prostate tumors and micrometastases. ACS Nano 2013;7(5):4221–32.
[100] Chen F, Hong H, Shi S, Goel S, Valdovinos HF, Hernandez R, et al. Engineering of hollow mesoporous silica nanoparticles for remarkably enhanced tumor active targeting efficacy. Sci Rep 2014;4:5080.
[101] Verel I, Visser GW, Boellaard R, Stigter-van Walsum M, Snow GB, van Dongen GA. ^{89}Zr immuno-PET: comprehensive procedures for the production of ^{89}Zr-labeled monoclonal antibodies. J Nucl Med 2003;44(8):1271–81.
[102] Holland JP, Sheh Y, Lewis JS. Standardized methods for the production of high specific-activity zirconium-89. Nucl Med Biol 2009;36(7):729–39.
[103] Holland JP, Williamson MJ, Lewis JS. Unconventional nuclides for radiopharmaceuticals. Mol Imaging 2010;9(1):1–20.

[104] Holland JP, Caldas-Lopes E, Divilov V, Longo VA, Taldone T, Zatorska D, et al. Measuring the pharmacodynamic effects of a novel Hsp90 inhibitor on HER2/neu expression in mice using ^{89}Zr-DFO-trastuzumab. PLoS ONE 2010;5(1):e8859.
[105] Holland JP, Divilov V, Bander NH, Smith-Jones PM, Larson SM, Lewis JS. ^{89}Zr-DFO-J591 for immunoPET of prostate-specific membrane antigen expression in vivo. J Nucl Med 2010;51(8):1293–300.
[106] Ruggiero A, Villa CH, Holland JP, Sprinkle SR, May C, Lewis JS, et al. Imaging and treating tumor vasculature with targeted radiolabeled carbon nanotubes. Int J Nanomedicine 2010;5:783–802.
[107] Lee J, Lee TS, Ryu J, Hong S, Kang M, Im K, et al. RGD peptide-conjugated multimodal $NaGdF_4$:Yb^{3+}/Er^{3+} nanophosphors for upconversion luminescence, MR, and PET imaging of tumor angiogenesis. J Nucl Med 2013;54(1):96–103.
[108] Lijowski M, Caruthers S, Hu G, Zhang H, Scott MJ, Williams T, et al. High sensitivity: high-resolution SPECT-CT/MR molecular imaging of angiogenesis in the Vx2 model. Invest Radiol 2009;44(1):15–22.
[109] Hu G, Lijowski M, Zhang H, Partlow KC, Caruthers SD, Kiefer G, et al. Imaging of Vx-2 rabbit tumors with $\alpha_v\beta_3$-integrin-targeted ^{111}In nanoparticles. Int J Cancer 2007;120(9):1951–7.
[110] Yang M, Cheng K, Qi S, Liu H, Jiang Y, Jiang H, et al. Affibody modified and radiolabeled gold-iron oxide hetero-nanostructures for tumor PET, optical and MR imaging. Biomaterials 2013;34(11):2796–806.